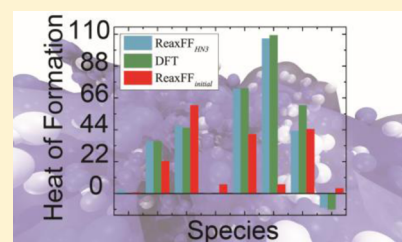


Reactive Force Field for Liquid Hydrazoic Acid with Applications to Detonation Chemistry

David Furman,^{†,||} Faina Dubnikova,[†] Adri C. T. van Duin,[‡] Yehuda Zeiri,^{§,||} and Ronnie Kosloff^{*,†}[†]Fritz Haber Research Center for Molecular Dynamics, Institute of Chemistry, Hebrew University of Jerusalem, Jerusalem 91904, Israel[‡]Department of Mechanical and Nuclear Engineering, Pennsylvania State University, University Park, Pennsylvania 16802, United States[§]Biomedical Engineering, Ben Gurion University, Beer-Sheva 94105, Israel^{||}Division of Chemistry, NRCN, P.O. Box 9001, Beer-Sheva 84190, Israel

S Supporting Information

ABSTRACT: The development of a reactive force field (ReaxFF formalism) for hydrazoic acid (HN₃), a highly sensitive liquid energetic material, is reported. The force field accurately reproduces results of density functional theory (DFT) calculations. The quality and performance of the force field are examined by detailed comparison with DFT calculations related to uni, bi, and trimolecular thermal decomposition routes. Reactive molecular dynamics (RMD) simulations are performed to reveal the initial chemical events governing the detonation chemistry of liquid HN₃. The outcome of these simulations compares very well with recent results of tight-binding DFT molecular dynamics and thermodynamic calculations. On the basis of our RMD simulations, predictions were made for the activation energies and volumes in a broad range of temperatures and initial material compressions.



1. INTRODUCTION

Hydrazoic acid, the simplest covalent azide-based material, is used as a source for imine radicals in organic synthesis¹ and serves as a reactant in gas-phase iodine lasers.² The limited use of HN₃ in organic synthesis is attributed to its highly unstable and explosive nature at room temperature.³ Nevertheless, it was demonstrated that HN₃ can be desensitized sufficiently in aqueous solutions so as to be safe to handle while still considered to be highly explosive.⁴ Owing to its simple molecular structure, HN₃ can serve as a model liquid system to study material properties and behavior under extreme conditions such as during detonation.^{5–7} In addition, HN₃ is the simplest template for more complex systems such as organic azides.^{8–11} Due to the existence of conjugated N=N=N bonds in the molecule, it is tempting to claim that polymerization and subsequent transition to a nonmolecular and even a metallic state may be possible following high pressure loading.¹² Although it was first synthesized in 1890, its crystal structure has only recently been determined experimentally and shows a unique network of hydrogen bonds.¹² Some elementary mechanistic studies were conducted for gas phase and highly diluted HN₃ aqueous solutions,^{13,14} however, the complete decomposition chemistry of the condensed phase deserves further investigation. To fully understand the reactive processes occurring during HN₃ decomposition under extreme conditions for long periods of time and large-scale systems, a new reactive force field parametrization has been developed based on the ReaxFF formalism.^{15–17} The study of shock and

detonation phenomena from an atomistic viewpoint requires large computational cells to permit a stable detonation wave propagation, and hence, classical molecular dynamics simulations are the method of choice. The ReaxFF methodology was chosen since it allows for the simulation of reactive systems with more than 10⁶ atoms, approaching the domain of micron-scale phenomena with near quantum mechanical accuracy. Although being approximate in its nature, this approach has been successfully used in recent years to study complex reactive systems with various applications, some of which include the characterization of processes occurring at the interfaces of hypergolic propellants,¹⁸ the study of water molecules dissociation on Titania surfaces,¹⁹ prediction of terahertz spectra of explosive crystals,²⁰ and detailed mechanistic studies of energetic materials in the condensed phase.^{21,17}

Starting from an existing ReaxFF parametrization proved to describe well nitramine and nitro-aromatic energetic materials,²² we have reparameterized the training set of bond dissociation energies, valence angles bending and dihedral rotations, heats of formation, lattice energies, reaction barriers, and enthalpies in all cases where solely nitrogen and hydrogen atoms are involved (i.e., optimization of the N/H chemistry). The force field is thus designed to reproduce a large “training set” based on accurate electronic structure (DFT) calculations.

Received: November 4, 2015

Revised: February 11, 2016

Published: February 17, 2016

The new force field is then evaluated and is subsequently used to predict the decomposition chemistry of liquid HN_3 at the experimental Chapman-Jouguet (CJ) conditions ($T_{\text{CJ}} = 4600$ K, $P_{\text{CJ}} = 16$ GPa). The results are compared to recent tight-binding simulations and thermochemical calculations. Further studies at a broad range of temperature and compression are carried out to fully characterize the decomposition process and kinetics.

2. COMPUTATIONAL DETAILS

2.1. Density Functional Theory Calculations. DFT calculations were performed to generate a database of different chemical structures and energies related to N/H chemistry. The calculations employed the CAM-B3LYP²³ hybrid DFT functional with the aug-cc-pVTZ basis set.²⁴ This combination yields results that compare well with energy barriers calculated using the highly accurate CBS/MRCI(Q) method in a recent study²⁵ of HN_3 low-lying states. All calculations were carried out using the Gaussian-09²⁶ package. The vibrational analysis of the structures was performed at the same level of theory to characterize the optimized structures as local minima or transition states. All the calculated frequencies, the zero-point energies, and the thermal energies correspond to the use of harmonic approximation. Intrinsic reaction coordinates calculation using internal coordinates was performed to examine whether the considered transition states connect the expected reactants and products. The thermal decomposition routes examined included single, two, and three HN_3 molecules as a starting point for the calculations.

2.2. ReaxFF Force Field. Developed from first-principles concepts, ReaxFF is a force field based on bond-order description and has been used to model atomistic scale molecular dynamics of reactive chemical systems in numerous applications. Unlike classical force fields, ReaxFF allows the description of bond formation and rupture events on the fly. The method was developed with the goal to reproduce accurately costly quantum mechanical (QM) data for large variety of reactants and products, including reactive intermediates and transition states. ReaxFF employs a set of potential energy functions that incorporate a large set of adjustable parameters. The parameters are optimized to reproduce the potential energy surfaces of reactive species found in more accurate QM calculations. This allows the modeling of dynamical processes in systems far too large to handle using QM calculations and for much longer times. The potential energy function used in ReaxFF has the following terms (eq 1):

$$E_{\text{system}} = E_{\text{bond}} + E_{\text{val}} + E_{\text{tors}} + E_{\text{over}} + E_{\text{under}} + E_{\text{pen}} + E_{\text{conj}} + E_{\text{vdW}} + E_{\text{Coulomb}} \quad (1)$$

In eq 1, the first three terms correspond to valence interactions and are responsible for bond energies, valence angle, and torsion angle. The next four terms include correction of over and under coordination of atoms, a penalty term accounting for double bond valence angle energy, angle conjugation energy, and the last two terms are long-range van der Waals and Coulomb interactions calculated for each pair of atoms independent of bond order. The instantaneous atomic charges are calculated with the EEM charge equilibration method²⁷ that takes into account the local environment and the geometry of the molecule. The training procedure starts with

extensive calculations of QM data related to reaction barriers and enthalpies, including transition states and intermediate structures, energies of stable and reactive species composed of H and N atoms including HN_3 , NH_3 , N_2 , H_2 , N_2H_4 , N_2H_2 , HN_2 , and others. Next, optimization of the force field is carried out. The training of the parameters is done via a single parameter search optimization²⁸ to minimize the following sum of squares (eq 2):

$$\text{Error} = \sum_{i=1}^n \left[\frac{(x_{i,\text{QM}} - x_{i,\text{ffield}})}{\sigma} \right]^2 \quad (2)$$

where $x_{i,\text{QM}}$ is the QM value, $x_{i,\text{ffield}}$ is the ReaxFF value, and σ is the weight (accuracy) specified in the training set. During the reparameterization procedures, we kept fixed all existing parameters concerning C/H/O atoms. These parameters were taken to be identical to those in Zhang et al.²⁹ suitable for nitramines. These parameters were kept intact to account for already parametrized interactions, such as N=O bond dissociation, N–H bond dissociation, bond angles (H–NH–H, H–O–NH₂, HO–NH–OH, H₂N–NH–NH₂, and O=N–NH₂, etc.), reaction enthalpies for nitramine decomposition channels (RDX, PETN, NM, and TATB), and various H-bond transfer reactions. We have augmented the force field with additional relevant energetics data, including bond dissociation paths of HN_3 , angles and torsions energetics, transition states, and intermediates of key N/H reaction steps, lattice energies, and heats of formation, partial atomic charges, and geometry data (equilibrium bond lengths and angles), as will be presented in the results.

2.3. Thermal Decomposition Simulations. To study the mechanism of the thermal decomposition of HN_3 at CJ conditions, the temperature and pressure were maintained at their CJ values ($T_{\text{CJ}} = 4600$ K, $P_{\text{CJ}} = 16$ GPa) during the simulation in NPT ensemble. All simulations were carried out using the open source LAMMPS³⁰ package. The first stage in the simulation is energy minimization where the atomic positions of 256 HN_3 molecules that were placed inside a rectangular box with dimensions $26.12 \times 26.12 \times 26.54$ Å were optimized using periodic boundary conditions. Next, a thermal equilibration step was performed for 10 ps to obtain thermalized atomic positions using a Berendsen³¹ thermostat at $T = 250$ K, between the melting and boiling points of HN_3 ($T_{\text{m}} = 193$ K, $T_{\text{b}} = 310$ K) with a coupling parameter of 25 fs and a time step of 0.25 fs. To reduce any artificial stress and obtain the equilibrated structure at ambient pressure, a subsequent pressure equilibration step was carried out using a Nose-Hoover thermostat/barostat combination.³² The system was equilibrated at $P = 1$ atm and $T = 300$ K for additional 20 ps with coupling constants of 25 and 250 fs for the temperature and pressure, respectively. At the final stage, an ambient system (cell volume $V = V_0 = 1.7 \times 10^{-20}$ cm³) was obtained with density of $d_0 = 1.06$ gr/cm³, in excellent agreement with the experimental density of the liquid at room temperature of 1.09 gr/cm³. The thermal decomposition simulation at CJ conditions was initiated at this point by applying constant high temperature and pressure conditions (isothermal–isobaric ensemble), and maintaining an average temperature and pressure of 4600 K and 16 GPa. The thermal decomposition simulation was carried out for 50 ps with a shorter time step of 0.1 fs to adequately account for fast vibrational modes at these conditions. To study the influence of different initial compressions and decomposition temperatures on the thermal

decomposition process, the ambient system (V_0) was adjusted to generate two initially highly compressed systems ($V/V_0 = 0.8$ and $V/V_0 = 0.7$). The thermal decomposition simulations of the three systems $V_0 - 0.7 V_0$ at temperatures in the range of 2600–4600 K were conducted using the NVT ensemble. During all simulations, the instantaneous bond order between each pair of atoms was monitored and properly averaged (using every 10 instantaneous bond-order values, 10 fs apart) to prevent artificial bonds identification during possibly very short high density encounters. The thermodynamic parameters and chemical bonds data were stored every 100–1000 fs.

3. RESULTS

3.1. Validation of ReaxFF_{HN3} Force Field. The initial force field used in the training procedure was designed to accurately reproduce energies obtained in DFT calculations of nitramines and nitro-aromatic explosives (NM, RDX, TATB, PETN, and HMX) and is based on a large set of DFT data.²² However, as expected, this force field performance for the study of liquid HN₃ was rather poor. Since no data regarding azide chemistry was incorporated in the original training set, the resulting force field was unable to accurately describe the polarizabilities, geometries, ambient density, and other important energy values associated with the chemistry of hydrazoic acid and related compounds. Figure 1 presents the

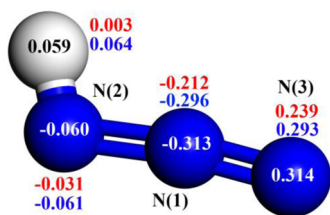


Figure 1. Partial atomic charges of HN₃: Mulliken-DFT (BW), ReaxFF_{HN3} (blue), and ReaxFF_{initial} (red).

partial atomic charges obtained in DFT (CAM-B3LYP/cc-pVTZ) using the Mulliken population analysis. Local electronegativity is described well by Mulliken charges which offer a self-consistent scheme for obtaining partial atomic charges. Mulliken charges are well-behaved for similar systems, and the method is well-suited for fitting electronegativity and hardness parameters in the EEM³³ scheme implemented in the ReaxFF training procedure.

The hydrogen atom in hydrazoic acid is nearly electrically neutral, bearing a charge of (+0.059e). The trained ReaxFF_{HN3} force field predicts a slightly larger value (+0.064e), while the

initial, nitramines-based force field, deviates markedly with the value of +0.003e. The nitrogen atom bonded to the hydrogen is compensating for the positive charge, with a negative charge of −0.060e. This compares well to the value assigned by ReaxFF_{HN3} (−0.061e), while the initial force field yields a reduced value (−0.031e). The other two nitrogen atoms show better agreement, again with the new force field performing much better than the initial one in reproducing the DFT values.

A correct description of bonding in molecular materials is important for accurate implementation of reactive force fields, where bond formation and rupture events can occur with high frequency during the simulation. The near-equilibrium values of bonds are required with high accuracy to enable a correct description of bonding nature at ambient conditions, while the far extreme ends are responsible for correct dissociation limits and high pressure environmental conditions often encountered in shocks and detonations. The description of all bonds in HN₃ has been improved as can be seen in Figure 2. The DFT calculations were performed with both spin singlet and triplet spin states to better represent the correct behavior. However, since ReaxFF has no unique energy terms for different spin states, the methodology used here is to train the force field at each internuclear separation with respect to the lowest-lying potential energy curve. The H–N(2) bond potential energy curve as reproduced by the trained force field is in much better agreement with the DFT results near the dissociation limit, while in near equilibrium bond separation, the DFT data is described equally well by both force fields. The N(1)–N(2) bond is better described with the ReaxFF_{HN3} force field near equilibrium, while both force fields show similarly good agreement, compared to DFT values, for the N(2)–N(3) bond.

Next, the angular dependence was examined. In most cases, much lower energies are obtained compared to those of valence bonds. As can be seen in Figure 3 the ReaxFF_{HN3} outperforms the unmodified force field. The H–N–N angle deviates strongly for angles above $\sim 110^\circ$ and exhibit a minimum value around 105.34° compared to 110.51° in ReaxFF_{HN3} and 110.34° in the DFT results. The other valence angle, N–N–N, is “softer” and shows similar behavior with a slightly better description by ReaxFF_{HN3}. The equilibrium values obtained are 172.17° , 169.54° , and 172.45° for ReaxFF_{HN3}, ReaxFF_{initial}, and DFT, respectively.

Figure 4 shows the heats of formation of various N_nH_m species relevant to liquid HN₃ decomposition chemistry. The values in Figure 4 compare the results of the DFT calculations with those of ReaxFF_{HN3} and the initial force field, ReaxFF_{initial}. The heat of formation is a basic thermochemical quantity characterizing the material’s stability relative to its constituent

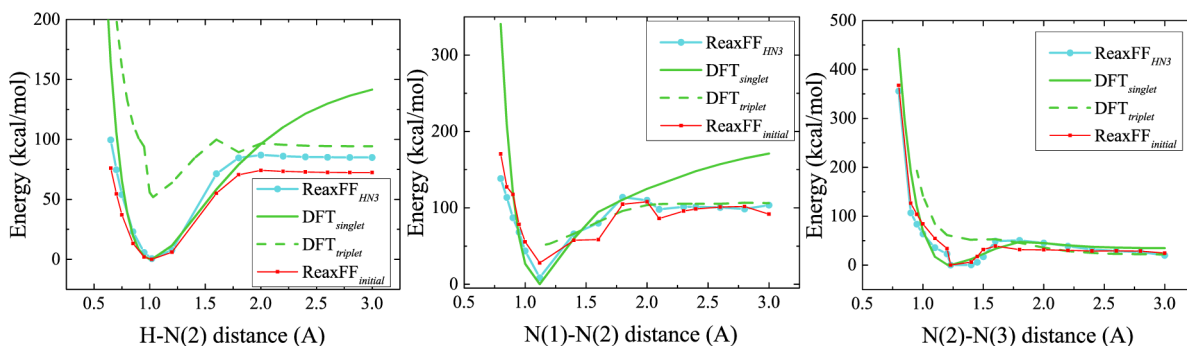


Figure 2. Bond dissociation curves of (left) H–N(2); (middle) N(1)–N(2); and (right) N(2)–N(3) in HN₃.

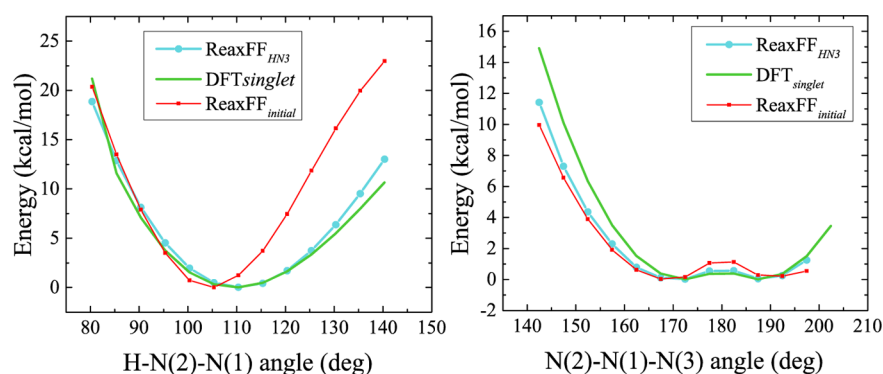


Figure 3. (Right) N(2)–N(1)–N(3) and (left) H–N(2)–N(1) angles bending curve in HN_3 .

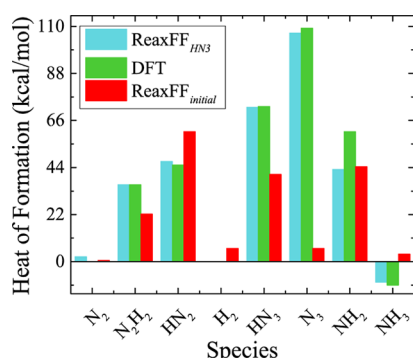


Figure 4. Heats of formation (kcal/mol) for various N/H species.

elements. The initial force field used in the training procedure lacks the ability to accurately differentiate between related N/H compounds, thus N_3 radical, a highly unstable species, is predicted to have a small positive heat of formation, while HN_3 which is a stable molecule yields a higher positive heat of formation. Another unrealistic prediction of the initial force field is of a positive heat of formation for ammonia, where, in fact, it should have a negative value of approximately -11 kcal/mol.³⁴ Using $\text{ReaxFF}_{\text{HN}_3}$ markedly improves the results. N_3 radical becomes less stable with a highly positive value (~ 100 kcal/mol) showing good agreement with DFT results. The predicted heat of formation for HN_3 is almost identical to that predicted by DFT, and the correct sign and value are predicted for ammonia.

The heat of formation is an important constituent of the training set. However, many other energy values should be embedded in the force field to expand its accuracy in describing reaction paths, intermediates, transition states, and general scope of applicability. Thus, we have conducted extensive reaction path calculations of uni-, bi-, and trimolecular total energies of key reactions using DFT calculations and trained the force field to reproduce all these quantities. A partial list of these reactions is presented in Figure 5 together with the force field predicted energies.

The thermal decomposition of HN_3 has been studied in the past both experimentally^{14,5} and computationally.^{6,7} The experimental efforts were limited to dilute HN_3 in argon, thus, the applicability of their results is limited to the gas phase. In accordance with our DFT calculations, the more favorable unimolecular decomposition channel, namely, the one with the lowest barrier ($\Delta E_{\text{r}} = 16.39$ kcal/mol) is the spin-forbidden channel forming the triplet ^3NH , in agreement with literature.^{5,14} $\text{ReaxFF}_{\text{HN}_3}$ was trained to reproduce the energy

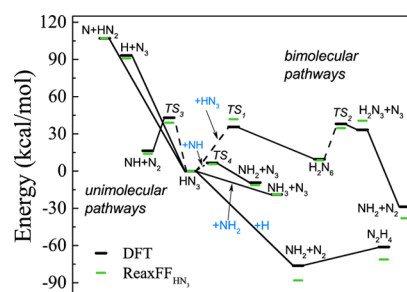


Figure 5. HN_3 decomposition pathways obtained with $\text{ReaxFF}_{\text{HN}_3}$ (green lines) and DFT calculations (black lines). Dashed lines represent transition states.

barrier of the lowest energy route (i.e., the spin-forbidden channel). Kajimoto et al.¹⁴ and Knyazev et al.⁵ analyzed the kinetics of secondary reactions in shock tube experiments and identified several possible decomposition and recombination reactions. Some of the key reactions in Figure 5 are based on their suggestions. The three main unimolecular decomposition channels of HN_3 in the gas phase (Figure 5, top left) are reproduced with excellent agreement with deviation of at most ~ 2 kcal/mol compared to DFT. Furthermore, according to our DFT calculations, among the three unimolecular decomposition pathways, the reactions leading to $\text{H} + \text{N}_3$ and $\text{N} + \text{HN}_2$ are barrierless with reaction energies of 90.9 and 106.9 kcal/mol, respectively. These values are in excellent agreement with recent highly accurate CBS/MRCI(Q) calculations.²⁵ The decomposition to produce $\text{NH} + \text{N}_2$ proceeds with a barrier (TS3) of 43.0 kcal/mol, in good agreement with the value of 43.9 kcal/mol, obtained in the CBS/MRCI(Q) study.²⁵ In condensed phases, the close proximity of adjacent molecules, in the crystalline or liquid phases, increase the probability of fruitful bimolecular encounters. Thus, it is of great importance to include bimolecular pathways in the training set for the simulations of condensed phase chemistry. Our preliminary thermal decomposition simulations indicated that the fruitful collision of two HN_3 molecules starts the decomposition sequence, hence we have identified the transition states and energy barriers for reactive events between two HN_3 molecules using DFT calculations. In accordance with this decomposition pathway, two HN_3 molecules collide to generate H_2N_6 , a metastable intermediate, via a transition state (TS1) located 35.5 kcal/mol above the reactants with endothermicity of 9.5 kcal/mol. In the second step, H_2N_6 decomposes into H_2N_3 and N_3 via a second transition state (TS2) with $\Delta E^\ddagger = 33.5$ kcal/mol and reaction energy of +33.3 kcal/mol. The force field was then trained to accurately reproduce this two-step decom-

position route. As can be inferred from Figure 5, the force field nicely reproduces the activation barriers and reaction energies for the first step ($\Delta E_{TS1}^\ddagger = 41.8$ kcal/mol and $\Delta E_1 = 8.7$ kcal/mol) and second step ($\Delta E_{TS2}^\ddagger = 30.8$ kcal/mol and $\Delta E_2 = 40.6$ kcal/mol). Additional primary and secondary condensed phase channels related to HN_3 decomposition have been included in the training set, as is seen in Figure 5. With respect to this set of reactions, the initial nitramines force field performed poorly, predicting opposite signs of reaction energies for several reactions. Specifically, it erroneously predicts that the association of two HN_3 molecules to form the H_2N_6 intermediate releases 13.5 kcal/mol, in contrast to the endothermic (+9.5 kcal/mol) value predicted by DFT. Moreover, the production of H_2N_3 and N_3 radicals from two HN_3 molecules is predicted to be -6.7 kcal/mol, compared to the DFT value of -38.1 kcal/mol. Thus, the bimolecular paths examined were not reproduced with sufficient accuracy, invalidating the initial nitramine force field predictions in condensed phase HN_3 . In the case of unimolecular reactions, deviations of up to 10–20 kcal/mol were observed for $\text{ReaxFF}_{\text{initial}}$. For example, the unimolecular decomposition channel of HN_3 leading to $\text{H} + \text{N}_3$ is predicted to be 76 kcal/mol compared to the DFT value of 93.2 kcal/mol. Although the newly developed $\text{ReaxFF}_{\text{HN}_3}$ accurately reproduces both the unimolecular and bimolecular reaction channels, its transferability toward nitramine and nitroaromatic chemistry was tested so to make sure the tuning of the N/H chemistry did not alter the already optimized terms.

Figure 6 shows the reaction energies in the training data to the original nitramines force field, $\text{ReaxFF}_{\text{initial}}$. As can be seen,

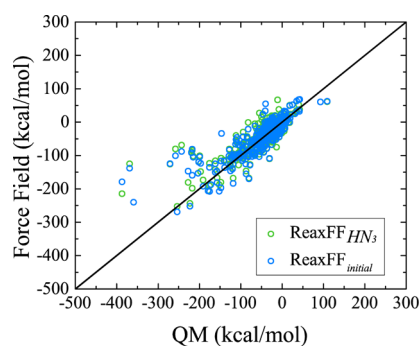
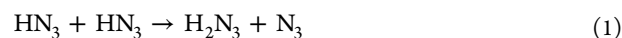


Figure 6. Performance comparison between $\text{ReaxFF}_{\text{HN}_3}$ and initial nitramines force field with respect to QM data used to train the latter. Values represent reaction energies in the training set.

the points are distributed along a straight line, in good agreement with the nitramine optimized force field. The data in Figure 6 proves that the new force field is transferable and equally adequate to describe nitramine and nitroaromatic explosives, in addition to hydrazoic acid and related materials.

3.2. Thermal Decomposition of Liquid HN_3 at Simulated CJ Conditions. The force field reported in this work was tested against and compared with the predictions of the decomposition processes occurring as a result of a thermal insult. A super cell containing 256 HN_3 molecules representing liquid HN_3 (300 K, $d = 1.06\text{gr}/\text{cm}^3$) was subjected to constant temperature and pressure conditions, characterizing the experimental Chapman-Jouguet point⁴ ($T_{\text{CJ}} = 4600\text{K}$, $P_{\text{CJ}} = 16$ GPa). These conditions were achieved using a Nose-Hoover thermostat and barostat, as described in section 2.3. Figure 7 presents the most prevalent species (>5% of initial HN_3 amount) formed during the liquid HN_3 decomposition process and the corresponding potential energy curve. Inspection of the potential energy evolution as a function of time shows that the first few picoseconds of the thermal decomposition are clearly strictly endothermic, reaching a maximum value of potential energy at ~ 2.5 ps. This is the period during which most of the bond breaking occurs, retaining minor amounts of the initial reactant molecules. The potential energy profile reaches a plateau after merely 10 ps, indicating that a quasi-steady state has been reached in which the amounts and identities of decomposition products remain practically constant. This is in excellent agreement with the results of Reed et al.⁶ who used a self-consistent charge tight-binding molecular dynamics to simulate detonation of liquid HN_3 at the C-J conditions. Close inspection of the variation of different decomposition products as a function of time (Figure 7) reveals that the decomposition of liquid HN_3 begins with the following reactions:



Reaction 1 proceeds via 2 transition states (identified by DFT) and H_2N_6 as intermediate, and it has larger contribution than reactions 2 and 3. This pathway generates a substantial amount of H_2N_3 that reaches a maximum value at about 0.45 ps, before other reactions result in the disappearance of these intermediate species. The formation of N_2 begins after about 0.3 ps and is attributed mainly to H_2N_3 decomposing into NH_2

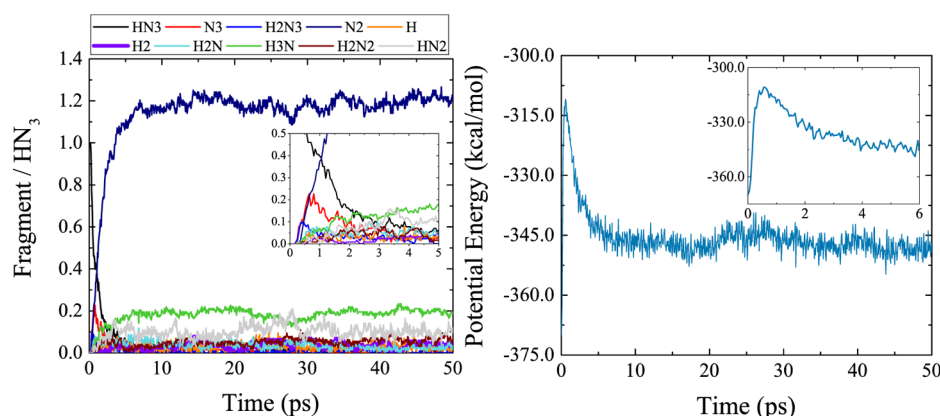


Figure 7. Species evolution during decomposition of HN_3 at the CJ conditions (left) and the associated potential energy (right).

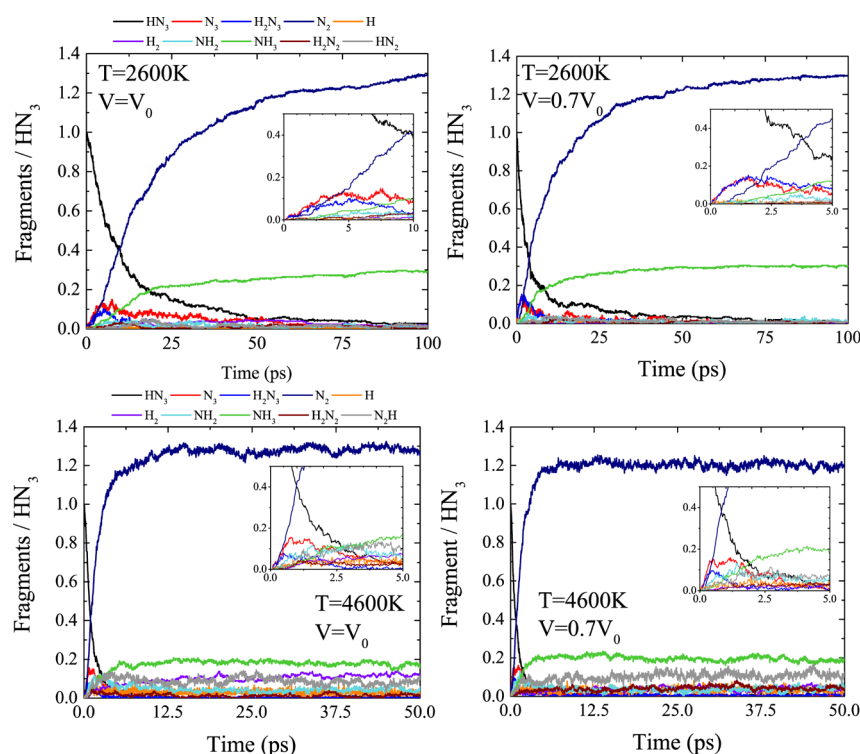


Figure 8. Thermal decomposition in various low and high temperatures and densities of HN_3 .

and N_2 and the direct decomposition of HN_3 to NH and N_2 which proceeds with a high-energy transition state ($\Delta E^\ddagger = 44.6$ kcal/mol). The production of ammonia begins together with the formation of N_2 although with a much slower rate. The N_3 radical is the most prevalent intermediate reaching a maximum value at approximately 0.65 ps and then decreasing to negligible amounts during the next 2 ps. We find that the stable species in the decomposition are N_2 and NH_3 with minor amounts (<10%) of H_2 and H . The calculated relative amounts of each of the stable final products relative to the initial amount of HN_3 are 1:1.2:0.2:0.05 for $\text{HN}_3:\text{N}_2:\text{NH}_3:\text{H}_2$, respectively. The reported ratios from tight-binding DFT and CHEETA thermochemical calculations (Reed et al.) are 1:1.3:0.3:0.02 and 1:1.4:0.2:0.2, respectively. Thus, it is demonstrated that $\text{ReaxFF}_{\text{HN}_3}$ reach a near QM accuracy for the description of the decomposition chemistry of HN_3 .

3.3. Effects of Temperature and Density on Decomposition Kinetics. To assess the effect of high material compression on the decomposition of liquid HN_3 , additional simulations were carried out. The minimized computational cell at ambient conditions (V_0) was adjusted by remapping the atomic coordinates so to obtain 2 additional systems at high initial compressions: $0.8V_0$ and $0.7V_0$. These configurations are 25% and 42% denser than the ambient system, respectively. The three systems were then equilibrated at 300 K for 10 ps. Thermal decomposition simulations followed in the canonical ensemble (NVT) at a specified target temperature using the Berendsen thermostat. In order to extract kinetic parameters, each system was simulated at 3 temperatures: 2600, 3600, and 4600 K. Thus, a total of 9 cases varying in combinations of density and temperature are accounted for. Figure 8 presents only the results of the extreme cases: lowest temperature (2600 K) and density (V_0) and highest temperature (4600 K) and density ($0.7V_0$).

The major difference between the four cases presented in Figure 8 is related to the effect of temperature on the rate of decomposition. The type of intermediate products and final stable species generated do not seem to be affected by variation of the decomposition temperature. Hence, it seems that the thermal decomposition mechanism does not change in the temperature range of 2600–4600 K. For low temperature $T = 2600$ K and ambient density, the complete disappearance of parent HN_3 molecules occur after nearly $t = 100$ ps, while at $T = 4600$ K, the complete decomposition is observed at approximately $t = 10$ ps, an order of magnitude faster. In addition, high decomposition temperatures lead to production of larger amounts of ammonia, H_2 , and N_2H . Pressure can have an important role in the decomposition of explosives. For example, bimolecular reactions tend to accelerate at high pressures and material compressions, while unimolecular reactions become slower. In the present case, the simulation at initial volume of $0.7V_0$ shows a slightly faster decomposition kinetics at both temperatures presented in Figure 8. The final relative amounts of stable decomposition products remain generally the same regardless of degree of compression. In all cases, the initial steps of decomposition start with the bimolecular reaction product H_2N_3 , as was observed in the simulated CJ decomposition case described above (section 3.2).

To quantitatively characterize the decomposition kinetics of liquid HN_3 , we have calculated the half-lives ($t_{1/2}$) of HN_3 from the time-dependent decomposition curve (Figure 8) for each temperature and compression. The half-lives were then substituted in the second-order initial decomposition rate equation (eq 3)

$$t_{1/2} = \frac{1}{k[A]_0} \quad (3)$$

where $t_{1/2}$ (ps) is half-life time, $[A]_0$ (a.u.) is the initial amount of HN_3 molecules and k (ps^{-1}) is the bimolecular rate constant.

We note that these are generalized rate constants, characterizing the initial decomposition process up to $t = t_{1/2}$. Table 1

Table 1. Rate Constants, k (ps^{-1}), for HN_3 Decomposition at Various Temperatures and Compressions

T (K)/ V	k (ps^{-1})		
	V_0	$0.8V_0$	$0.7V_0$
2600	5.8×10^{-4}	1.1×10^{-3}	1.7×10^{-3}
3600	2.3×10^{-3}	3.1×10^{-3}	4.7×10^{-3}
4600	4.3×10^{-3}	5.9×10^{-3}	6.7×10^{-3}

presents the rate constants obtained for the different cases examined. These rate constants allow one to fully characterize the rate-determining transition state by assessing the activation energies and volumes for the decomposition process since Arrhenius behavior is observed.

The magnitude of the activation parameters can be deduced from the following differential expressions:¹⁷

$$\left(\frac{\partial \ln k}{\partial \left(\frac{1}{T} \right)} \right)_P = -\frac{E_a}{R}; \quad \left(\frac{\partial \ln k}{\partial P} \right)_T = -\frac{\Delta V^\ddagger}{RT} \quad (4)$$

Plotting the logarithm of rate constants versus reciprocal temperature allows one to extract the activation energy from the slope, and in a similar manner, the activation volume can be obtained. The Arrhenius pre-exponential factors are deduced from the intercept with the vertical axis. Figure 9 presents the results of this analysis.

The effective activation volumes for all compression values (in terms of average pressure) are negative, indicating that a bimolecular reaction is the rate-limiting step. This is consistent with the detailed molecular decomposition mechanism described in the previous sections. The activation volumes range from $-2.63 - (-1.57) \text{ cm}^3/\text{mol}$. Experimental studies of HN_3 decomposition in the literature are limited to dilute gas phase conditions. Thus, no values for the activation volumes in condensed phase are available for comparison. However, literature³⁵ data is available for common high explosives such as α -RDX ($-5.6 \text{ cm}^3/\text{mol}$), β -RDX ($+3.89 \text{ cm}^3/\text{mol}$), and β -HMX ($+4.1 \text{ cm}^3/\text{mol}$). Our values are smaller in magnitude as can be expected, since the size of the molecular structures in the transition state are much smaller compared to the nitramine explosive systems. The effective activation energies for liquid HN_3 decomposition are predicted to be in the range of 16.3–

23.9 kcal/mol in the compression range $0.7V_0 - V_0$. Arrhenius pre-exponential factors calculated from the intercept of Figure 9 (right): $\ln(A[\text{s}^{-1}]) = 24.83 \pm 0.17$, 24.62 ± 0.08 , and 24.47 ± 0.26 for V_0 , $0.8V_0$, and $0.7V_0$ systems, respectively. Higher initial material compressions result in lower-activation barriers and faster kinetics.

4. CONCLUSIONS

A new reactive force-field based on the ReaxFF formalism has been developed (ReaxFF_{HN3}) to adequately describe the chemistry under extreme conditions of liquid hydrazoic acid. Extensive electronic structure calculations were conducted to characterize the possible decomposition routes and secondary reactions and to train the force field. ReaxFF_{HN3} reproduces all major decomposition routes, heats of formation, and partial charges. It is shown to be in excellent agreement with previous results based on tight-binding DFT and thermochemical calculations using CHEETA code. The transferability of ReaxFF_{HN3} has been tested on a training set of nitramine and nitroaromatic energetic materials and was found to be consistent to adequately describe both azide and nitramine chemistry. It is revealed that the decomposition of liquid HN_3 begins with the formation of H_2N_3 and N_3 radicals via a twostep bimolecular route, contrary to many popular nitramine energetic materials, whose decomposition proceeds in a unimolecular channel. N_2 is the most stable species obtained in the decomposition process with lesser amounts of NH_3 . Further simulations of decomposition under wide range of temperatures and initial material compressions shed light on the high-pressure decomposition of liquid HN_3 . It is revealed that pressure plays an important role accelerating the decomposition; however, it does not alter the chemical mechanistic steps of decomposition. The complete decomposition of HN_3 takes 100 ps at 2600 K, and merely 10 ps at 4600 K at simulated CJ conditions, in excellent agreement to tight-binding DFT simulations. We find the effective activation energies to be in the range of 16.31–23.93 kcal/mol in the compression range $0.7V_0 - V_0$ and activation volumes in the range of $-2.63 - (-1.57) \text{ cm}^3/\text{mol}$ in the temperature range of 2600–4600K, respectively. Careful experimental studies of the decomposition of liquid HN_3 could verify our predictions. This study serves as the first step in establishing ReaxFF to simulate azide-based chemistry, allowing near QM accuracy at a highly reduced computational cost compared to ab initio or tight-binding DFT methods.

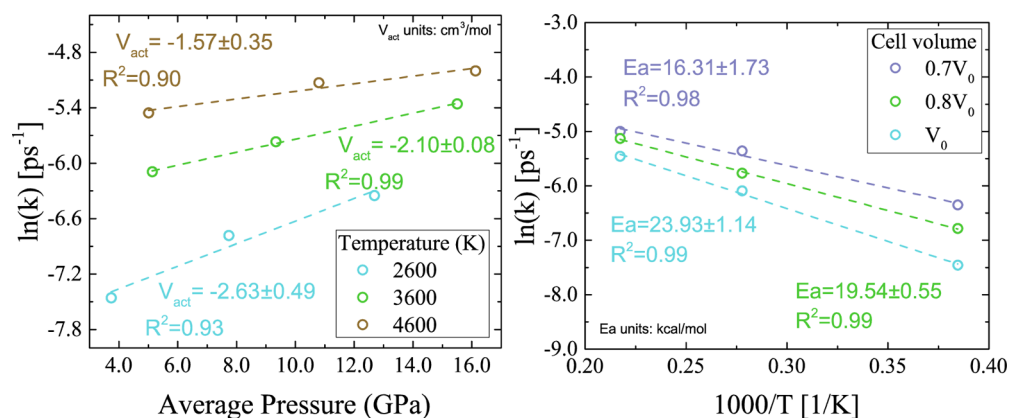


Figure 9. Rate constants for HN_3 decomposition versus average pressure (left) and versus reciprocal temperature (right).

■ ASSOCIATED CONTENT

● Supporting Information

The Supporting Information is available free of charge on the ACS Publications website at DOI: 10.1021/acs.jpcc.5b10812.

Reactive MD-force field (PDF)

■ AUTHOR INFORMATION

Corresponding Author

*E-mail: ronnie@fh.huji.ac.il

Notes

The authors declare no competing financial interest.

■ ACKNOWLEDGMENTS

This material is based upon work supported by the U.S. Department of Homeland Security, Science and Technology Directorate, Office of University Programs, under Grant 2013-ST-061-ED0001. The views and conclusions contained in this document are those of the authors and should not be interpreted as necessarily representing the official policies, either expressed or implied, of the U.S. Department of Homeland Security.

■ REFERENCES

- (1) Richards, Wc; Setser, D. W. Thermal Decomposition of Hydrazoic Acid as a Possible Source of Nh Radicals. *Can. J. Chem.* **1969**, *47*, 2725–2727.
- (2) Tang, S. K.; Duo, L. P.; Jin, Y. Q.; Yu, H. J.; Wang, J.; Sang, F. T. Study on Hn3 Production for All Gas-Phase Iodine Laser - Art. No. 63463l. *Proc. SPIE* **2006**, *6346*, L3463–L3463.
- (3) Wiss, J.; Fleury, C.; Heuberger, C.; Onken, U.; Glor, M. Explosion and Decomposition Characteristics of Hydrazoic Acid in the Gas Phase. *Org. Process Res. Dev.* **2007**, *11*, 1096–1103.
- (4) Kurbangalina, R. K.; Patskov, E. A.; Stesik, L. N.; Yakovleva, G. S. Detonation of Liquid Hydrazoic Acid and Its Aqueous Solutions. *J. Appl. Mech. Tech. Phys.* **1973**, *11*, 672–677.
- (5) Knyazev, V. D.; Korobeinichev, O. P. Thermal Decomposition of Hn3. *J. Phys. Chem. A* **2010**, *114*, 839–846.
- (6) Reed, E. J.; Rodriguez, A. W.; Manaa, M. R.; Fried, L. E.; Tarver, C. M. Ultrafast Detonation of Hydrazoic Acid (Hn3). *Phys. Rev. Lett.* **2012**, *109*, 0383011–0383015.
- (7) Reed, E. J. Electron-Ion Coupling in Shocked Energetic Materials. *J. Phys. Chem. C* **2012**, *116*, 2205–2211.
- (8) Wu, B. D.; Zhou, Z. N.; Li, F. G.; Yang, L.; Zhang, T. L.; Zhang, J. G. Preparation, Crystal Structures, Thermal Decompositions and Explosive Properties of Two New High-Nitrogen Azide Ethylenediamine Energetic Compounds. *New J. Chem.* **2013**, *37*, 646–653.
- (9) Brase, S.; Gil, C.; Knepper, K.; Zimmermann, V. Organic Azides: An Exploding Diversity of a Unique Class of Compounds. *Angew. Chem., Int. Ed.* **2005**, *44*, 5188–5240.
- (10) Gillan, E. G. Synthesis of Nitrogen-Rich Carbon Nitride Networks from an Energetic Molecular Azide Precursor. *Chem. Mater.* **2000**, *12*, 3906–3912.
- (11) Kubota, N. Combustion of Energetic Azide Polymers. *J. Propul. Power* **1995**, *11*, 677–682.
- (12) Evers, J.; Gobel, M.; Krumm, B.; Martin, F.; Medvedev, S.; Oehlinger, G.; Steemann, F. X.; Troyan, I.; Klapotke, T. M.; Eremets, M. I. Molecular Structure of Hydrazoic Acid with Hydrogen-Bonded Tetramers in Nearly Planar Layers. *J. Am. Chem. Soc.* **2011**, *133*, 12100–12105.
- (13) Foy, B. R.; Casassa, M. P.; Stephenson, J. C.; King, D. S. Overtone-Excited Hn3(X1a') - Anharmonic Resonance, Homogeneous Linewidths, and Dissociation Rates. *J. Chem. Phys.* **1990**, *92*, 2782–2789.
- (14) Kajimoto, O.; Yamamoto, T.; Fueno, T. Kinetic Studies of the Thermal-Decomposition of Hydrazoic Acid in Shock-Waves. *J. Phys. Chem.* **1979**, *83*, 429–435.
- (15) van Duin, A. C. T.; Dasgupta, S.; Lorant, F.; Goddard, W. A. Reaxff: A Reactive Force Field for Hydrocarbons. *J. Phys. Chem. A* **2001**, *105*, 9396–9409.
- (16) Strachan, A.; van Duin, A. C. T.; Chakraborty, D.; Dasgupta, S.; Goddard, W. A. Shock Waves in High-Energy Materials: The Initial Chemical Events in Nitramine Rdx. *Phys. Rev. Lett.* **2003**, *91*, 098301–098304.
- (17) Furman, D.; Kosloff, R.; Dubnikova, F.; Zybin, S. V.; Goddard, W. A.; Rom, N.; Hirshberg, B.; Zeiri, Y. Decomposition of Condensed Phase Energetic Materials: Interplay between Uni- and Bimolecular Mechanisms. *J. Am. Chem. Soc.* **2014**, *136*, 4192–4200.
- (18) Liu, Y.; Zybin, S. V.; Guo, J. Q.; van Duin, A. C. T.; Goddard, W. A. Reactive Dynamics Study of Hypergolic Bipropellants: Monomethylhydrazine and Dinitrogen Tetroxide. *J. Phys. Chem. B* **2012**, *116*, 14136–14145.
- (19) Raju, M.; Kim, S. Y.; van Duin, A. C. T.; Fichthorn, K. A. Reaxff Reactive Force Field Study of the Dissociation of Water on Titania Surfaces. *J. Phys. Chem. C* **2013**, *117*, 10558–10572.
- (20) Katz, G.; Zybin, S.; Goddard, W. A.; Zeiri, Y.; Kosloff, R. Direct Md Simulations of Terahertz Absorption and 2d Spectroscopy Applied to Explosive Crystals. *J. Phys. Chem. Lett.* **2014**, *5*, 772–776.
- (21) Rom, N.; Hirshberg, B.; Zeiri, Y.; Furman, D.; Zybin, S. V.; Goddard, W. A.; Kosloff, R. First-Principles-Based Reaction Kinetics for Decomposition of Hot, Dense Liquid Tnt from Reaxff Multiscale Reactive Dynamics Simulations. *J. Phys. Chem. C* **2013**, *117*, 21043–21054.
- (22) Rom, N.; Zybin, S. V.; van Duin, A. C. T.; Goddard, W. A.; Zeiri, Y.; Katz, G.; Kosloff, R. Density-Dependent Liquid Nitro-methane Decomposition: Molecular Dynamics Simulations Based on Reaxff. *J. Phys. Chem. A* **2011**, *115*, 10181–10202.
- (23) Yanai, T.; Tew, D. P.; Handy, N. C. A New Hybrid Exchange-Correlation Functional Using the Coulomb-Attenuating Method (Cam-B3lyp). *Chem. Phys. Lett.* **2004**, *393*, 51–57.
- (24) Dunning, T. H. Gaussian-Basis Sets for Use in Correlated Molecular Calculations 0.1. The Atoms Boron through Neon and Hydrogen. *J. Chem. Phys.* **1989**, *90*, 1007–1023.
- (25) Galvao, B. R. L.; Varandas, A. J. C. Accurate Study of the Two Lowest Singlet States of Hn3: Stationary Structures and Energetics at the Mrci Complete Basis Set Limit. *J. Phys. Chem. A* **2013**, *117*, 4044–4050.
- (26) Frisch, M. J.; Trucks, G. W.; Schlegel, H. B.; Scuseria, G. E.; Robb, M. A.; Cheeseman, J. R.; Scalmani, G.; Barone, V.; Mennucci, B.; Petersson, G. A., et al. *Gaussian 09*, Gaussian, Inc.: Wallingford, CT, 2009.
- (27) Rappe, A. K.; Goddard, W. A. Charge Equilibration for Molecular-Dynamics Simulations. *J. Phys. Chem.* **1991**, *95*, 3358–3363.
- (28) van Duin, A. C. T.; Baas, J. M. A.; van de Graaf, B. Delft Molecular Mechanics: A New Approach to Hydrocarbon Force Fields. Inclusion of a Geometry-Dependent Charge Calculation. *J. Chem. Soc., Faraday Trans.* **1994**, *90*, 2881–2895.
- (29) Zhang, L. Z.; Zybin, S. V.; van Duin, A. C. T.; Dasgupta, S.; Goddard, W. A.; Kober, E. M. Carbon Cluster Formation During Thermal Decomposition of Octahydro-1,3,5,7-Tetranitro-1,3,5,7-Tetrazocine and 1,3,5-Triamino-2,4,6-Trinitrobenzene High Explosives from Reaxff Reactive Molecular Dynamics Simulations. *J. Phys. Chem. A* **2009**, *113*, 10619–10640.
- (30) Plimpton, S. Fast Parallel Algorithms for Short-Range Molecular-Dynamics. *J. Comput. Phys.* **1995**, *117*, 1–19.
- (31) Berendsen, H. J. C.; Postma, J. P. M.; Vangunsteren, W. F.; Dinola, A.; Haak, J. R. Molecular-Dynamics with Coupling to an External Bath. *J. Chem. Phys.* **1984**, *81*, 3684–3690.
- (32) Martyna, G. J.; Tobias, D. J.; Klein, M. L. Constant-Pressure Molecular-Dynamics Algorithms. *J. Chem. Phys.* **1994**, *101*, 4177–4189.

(33) Mortier, W. J.; Ghosh, S. K.; Shankar, S. Electronegativity Equalization Method for the Calculation of Atomic Charges in Molecules. *J. Am. Chem. Soc.* **1986**, *108*, 4315–4320.

(34) Chase, M., Jr NIST-JANAF Thermochemical Tables, Parts I and II. *J. Phys. Chem. Ref. Data* **1998**, *25*, 551.

(35) Peiris, S. M.; Piermarini, G. J. *Static Compression of Energetic Materials*; Springer: Berlin, 2009.